A Nucleotide-Dependent Conformational Switch Controls the Polymerization of Human IMP Dehydrogenases to Modulate their Catalytic Activity

David Fernández-Justel[1], Rafael Núñez[2], Jaime Martín-Benito[3], David Jimeno[4], Adrián González-López[1], Eva María Soriano[1], José Luis Revuelta[1] and Rubén M. Buey[1]

*1 - **Metabolic Engineering Group,** Dpto. Microbiología y Genética, Universidad de Salamanca, Campus Miguel de Unamuno, 37007, Salamanca, Spain*
*2 - **Centro de Investigaciones Biológicas (CIB),** Spanish National Research Council (CSIC), Ramiro de Maeztu 9, 28040 Madrid, Spain*
*3 - **Centro Nacional de Biotecnología (CNB),** Spanish National Research Council (CSIC), Darwin 3, 28039 Madrid, Spain*
*4 - **Instituto de Biología Molecular y Celular del Cáncer (CSIC-Universidad de Salamanca),** Campus Miguel de Unamuno, 37007 Salamanca, Spain*

***Correspondence to José Luis Revuelta and Rubén M. Buey:** Lab 233, Edificio Departamental, Campus Miguel Universidad de Salamanca, de Unamuno, 37007 Salamanca, Spain. revuelta@usal.es, ruben.martinez@usal.es*
https://doi.org/10.1016/j.jmb.2019.01.020
Edited by Georg Schulz

Abstract

Inosine 5′-monophosphate dehydrogenase (IMPDH) catalyzes the rate-limiting step in the *de novo* GTP biosynthetic pathway and plays essential roles in cell proliferation. As a clinical target, IMPDH has been studied for decades, but it has only been within the last years that we are starting to understand the complexity of the mechanisms of its physiological regulation. Here, we report structural and functional insights into how adenine and guanine nucleotides control a conformational switch that modulates the assembly of the two human IMPDH enzymes into cytoophidia and allosterically regulates their catalytic activity. *In vitro* reconstituted micron-length cytoophidia-like structures show catalytic activity comparable to unassembled IMPDH but, in turn, are more resistant to GTP/GDP allosteric inhibition. Therefore, IMPDH cytoophidia formation facilitates the accumulation of high levels of guanine nucleotides when the cell requires it. Finally, we demonstrate that most of the IMPDH retinopathy-associated mutations abrogate GTP/GDP-induced allosteric inhibition and alter cytoophidia dynamics.

Introduction

Inosine 5′-monophosphate dehydrogenase (IMPDH) is the enzyme that catalyzes the rate-limiting step in the *de novo* guanine nucleotide biosynthetic pathway, which plays a crucial role in the regulation of the cellular pools of purine nucleotides. Therefore, IMPDH is a key enzyme involved in the control of cell viability, division and proliferation. Indeed, IMPDH is the target of a diverse number of drugs presently used in clinical chemotherapy such as immunosupressors, antivirals, anticancer or antibiotics [1].

IMPDH is composed of an archetypal TIM barrel catalytic domain and a Bateman regulatory domain, which is inserted within a loop of the catalytic module. In solution, the basic units of most IMPDHs are homotetramers that can dimerize in different ways to form octamers or higher-order oligomers [2–7].

Using the IMPDH enzyme from the industrial fungus *Ashbya gossypii* as a model, we have recently reported a molecular mechanism by which purine nucleotides allosterically modulate the catalytic activity. The competition of adenine or guanine nucleotides for their binding sites within the regulatory Bateman domain controls a conformational switch that modulates the catalytic activity by shifting from extended to compacted IMPDH octamers. Extended, ATP-induced octamers are fully active, while the catalytic activity of GTP/GDP-induced compacted octamers is significantly reduced [6,7]. The relevance of this allosteric mechanism of regulation is stressed by the observation that most of the described missense mutations in

human IMPDH isoform 1 associated with severe retinopathies, such as retinitis pigmentosa and leber congenital amaurosis [8], map into the nucleotide binding sites of the Bateman regulatory domain. Based on these results, it was proposed that the retinopathy-associated mutations might interfere with nucleotide binding and disrupt the allosteric regulation of human IMPDH isoform 1, generating constitutively active IMPDH mutants, which is in agreement with the dominant hereditary character of these mutations [7].

Adding more complexity to the mechanisms of IMPDH regulation, the two human enzymes have been reported to polymerize into mesoscale intracellular assemblies such as purinosomes [9] and micrometric structures denoted as *rod and rings* or *cytoophidia* [4,10,11]. Thereby, human IMPDH, as well as CTP synthase (CTPS) and some other metabolic enzymes, possesses the particular ability to self-assemble into higher-order structures. This macromolecular organization has been suggested to modulate enzyme activity and play important roles in regulating cell metabolism by controlling intracellular nucleotide homeostasis [12,13]. The two human IMPDH enzymes, in response to intracellular guanine-nucleotide depletion, assemble into micron-length cytoophidia that disappear once the guanine-nucleotide levels are restored. Remarkably, the physiological functions of IMPDH cytoophidia remain unclear, although it has been reported that polymerization correlates with rapid cell proliferation [11,14,15]. Nonetheless, the *in vitro* reconstituted polymers show identical activity for polymerized and non-assembled human IMPDH isoform 2 [5]. To reconcile these results, it has been recently speculated that filamentous IMPDH might be more resistant to GTP/GDP inhibition, facilitating the intracellular accumulation of GTP when required [15], but no experimental evidence supporting this hypothesis has been obtained. Moreover, there is an evident lack of information regarding the structural details and the molecular mechanisms governing the dynamics of IMPDH cytoophidia assembly *in vitro*. Indeed, to our best knowledge, the *in vitro* reconstituted IMPDH filaments studied so far consist of a few particles organized into chains polymerized by a back-to-back assembly mechanism [2,4,5] that do not resemble the micrometer-long fibrillar IMPDH cytoophidia that are observed in cells [10,11,16–21].

In this study, we report the *in vitro* reconstitution of the assembly of the two human IMPDH enzymes into cytoophidia-like polymers and their structural and functional characterization. We show that micron-length human IMPDH cytoophidia-like structures spontaneously assemble *in vitro* under macromolecular crowding conditions in the absence of nucleotides but disassemble when either GTP or ATP is present in the solution, resembling what is observed within cells. The *in vitro* reconstituted IMPDH cytoophidia-like polymers are catalytically functional, with similar activity to non-assembled IMPDH, but they are significantly more resistant to GTP/GDP allosteric inhibition. Our results show that the cytoophidia dynamics and the allosteric regulation of the catalytic activity are tightly linked to the purine nucleotide-controlled conformational switch that we have previously reported for the *A. gossypii* fungal IMPDH [6,7]. They further provide a plausible structural mechanism for the nucleotide-dependent dynamics of cytoophidia assembly. Finally, we present the high-resolution crystal structures of human IMPDH isoform 2 complexed to GTP and GDP and demonstrate that most of the retinopathy-associated missense mutations map into the allosteric binding sites, altering nucleotide binding and subsequently abrogating GTP/GDP-induced allosteric inhibition of human IMPDH isoform 1. In addition, these mutations also alter cytoophidia dynamics, suggesting a potential pathological role for these assemblies that deserves to be further investigated.

Results

A nucleotide-controlled conformational switch operates in both human IMPDH isoforms

By using the IMPDH enzyme from the industrial fungus *A. gossypii,* we have recently reported a conformational switch that modulates the catalytic activity in response to the binding of purine nucleotides within the Bateman regulatory domain: adenine nucleotides (ATP, ADP and AMP) induce active IMPDH octamers in an extended (~115 Å long) conformation, while guanine nucleotides (GTP and GDP) induce inhibited octamers in a compact (~95 Å long) conformation [6]. Experimental evidence of the existence of this conformational switch in the isoform 2 of human IMPDH (HsIMPDH2) was recently reported by using electron microscopy (EM) on ATP and GTP-induced helical protofilaments [5]. Here, we have further investigated the nucleotide-conformational switch in both human IMPDH isoforms (HsIMPDH1 and HsIMPDH2) *in vitro* by using small-angle x-ray solution scattering (SAXS).

HsIMPDH1 and HsIMPDH2 wild-type proteins at the concentration used for the SAXS experiments (2.5 mg/mL) are mostly octamers in solution, but the addition of nucleotides induces stochastic oligomerization (see below) that results in poly-disperse solutions [2,4,5], which are not appropriate for SAXS analysis. Thereby, we made use of the missense mutation Y12A that has been previously reported to abrogate polymerization of HsIMPDH2 *in vitro* and in cultured cells [5]. Indeed, in the absence of nucleotides, HsIMPDH1-Y12A and HsIMPDH2-Y12A mutant enzymes remained as monodisperse tetramers in solution, as demonstrated by size-exclusion chromatography (Supplemental Fig. 1A). This observation

indicates that the octamers that exist in solution in the absence of nucleotides are most probably formed by the back-to-back interaction of the catalytic domains of two tetramers with a crucial role for residue Y12, as suggested in previous reports [2,5].

The addition of ATP or GDP to HsIMPDH1/2-Y12A induces the association of two tetramers to form octamers (Fig. 1A and B). Remarkably, the SAXS profiles of both human IMPDH isoforms resemble those described for the *A. gossypii* ATP or GDP-induced octamers (Supplemental Fig. 1B–D), demonstrating that the conformational switch previously proposed for the fungal *A. gossypii* AgIMPDH [6] is also present in both isoforms of the human IMPDH enzyme.

As shown in Supplemental Fig. 1E–F, ATP induces the formation of octamers more potently than GDP for both HsIMPDH1 and HsIMPDH2. Interestingly, significant differences are observed between both isoforms. In HsIMPDH1, the GDP-induced inhibition of the catalytic activity correlates with octamer compaction (Fig. 1C). In contrast, GDP-induced compact octamers of HsIMPDH2 are formed before inhibition occurs (Fig. 1D), highlighting mechanistic differences between both human isoforms that might be relevant *in vivo*. Nonetheless, when ATP is present in the solution, GDP-induced octamers of both HsIMPDH1 and HsIMPDH2 are formed before catalytic inhibition occurs (Fig. 1C and D).

In summary, our data show that the nucleotide-controlled conformational switch initially described for the *A. gossypii* enzyme also operates in both human IMPDH isoforms, where the binding of ATP or GDP induces octamers, formed by the interaction of the Bateman domains of two tetramers. The presence of adenine nucleotides in the solution induces octamers with an extended conformation that are catalytically active, while guanine nucleotides induce the compaction of these octamers, significantly inhibiting their enzymatic activity.

Retinopathy-associated mutations abrogate the allosteric inhibition of human IMPDH

To gain insights into the binding modes of purine nucleotides to the Bateman domain of human IMPDH, we attempted to obtain high-resolution structural information by x-ray crystallography. This issue is

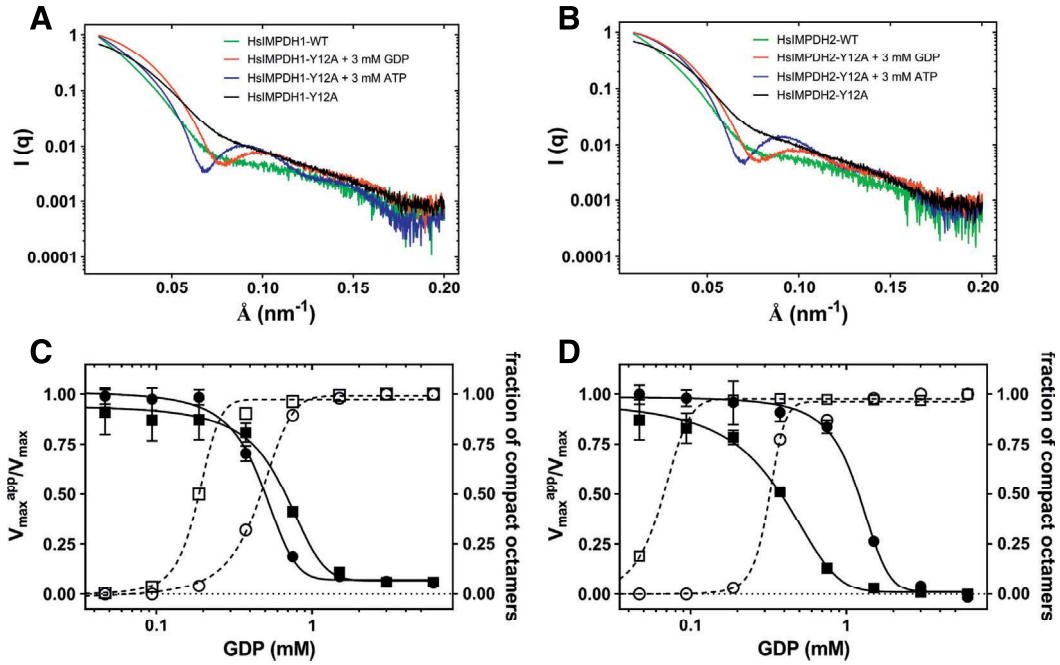

Fig. 1. The conformational switch of HsIMPDH controls its catalytic activity. (A and B) Experimental SAXS profiles of HsIMPDH1 (A) and HsIMPDH2 (B) wild-type and mutant Y12A (2.5 mg/mL) in the absence and presence of the indicated purine nucleotides. (C and D) Plots representing the fraction of compact octamers, as determined by SAXS, (empty symbols and dashed lines) and the catalytic activity (V_{max}^{app}/V_{max}; filled symbols and continuous lines) *versus* GDP concentration for HsIMPDH1-Y12A (C) and HsIMPDH2-Y12A (D). Squares: 3 mM ATP fixed concentration *versus* increasing concentrations of GDP. Circles: increasing concentrations of GDP in the absence of ATP. Data points represent the mean value and the standard errors. Lines represent the non-linear regression analysis of the experimental data, according to a standard allosteric sigmoidal equation (GraphPad Prism). At the fixed concentrations of ATP (3 mM) and GDP (3 mM) used for these experiments, HsIMPDH1-Y12A and HsIMPDH2-Y12A proteins remained as octamers with no detectable fraction of tetramers, as determined by SAXS.

especially relevant since, based on the *A. gossypii* fungal IMPDH structure, we have previously proposed that most of the retinopathy-associated missense mutations in HsIMPDH1 alter GTP/GDP-mediated allosteric inhibition [7]. Thereby, we solved the high-resolution crystal structures of HsIMPDH2 in complex with GTP and GDP, which are essentially identical (Supplemental Fig. 2A). A detailed description of these structures can be found in the Supplemental Information. Both structures unequivocally demonstrate that most of the retinopathy-associated mutations either (i) placed at the interface of two interacting Bateman domains: R224P, L227P and R231P (Supplemental Fig. 2C) or (ii) are directly involved in nucleotide binding at the allosteric sites of the Bateman domain: D226N for GTP/GDP2 (Supplemental Fig. 3B) and N198K and K238E for GTP3/GDP3 (Supplemental Fig. 3C).

We then introduced most of the missense mutations described in the literature [8] into HsIMPDH1 and purified the mutant enzymes for their analyses *in vitro*. Our results showed that the mutants had catalytic activity *in vitro* that fell within the same range (between 1.1- and 0.6-fold the activity of the WT; Fig. 2) as the WT enzyme. ATP showed no significant effect on the catalytic activity of both the WT and the mutant enzymes (between 1.0- and 0.6-fold the activity of the enzyme without nucleotide; Fig. 2). On the other hand, those mutations that map within the Bateman domain nucleotide binding sites (N198K, D226N and K238E; Supplemental Fig. 3) or at the interphase between the Bateman domains (R224P, L227P and R231P; Supplemental Fig. 2C) cannot be allosterically inhibited *in vitro* neither by GTP/GDP (Fig. 2), which thereby results in constitutively activated mutant enzymes.

In vitro reconstitution of micron-length human IMPDH cytoophidia assembly

We then investigated *in vitro* the ability of IMPDH to reversibly assemble into mesoscale structures that have been described to form within cells in response to the depletion of the intracellular guanine nucleotide pool [10,19,21]. It is important to stress here that several reports have shown that ATP and GTP induce the formation of IMPDH polymers *in vitro* [3–5], but these polymers consist of a few IMPDH octamers stacked back-to-back and organized into single filaments. Thereby, these polymers do not represent the IMPDH micron-length filamentous bundles that have been reported to form in cells [10,18,19,21].

These data suggest that an important factor is missing *in vitro*, but what could be this factor? An initial hint came from the published purification protocol of recombinant human IMPDH enzymes from *Escherichia coli* [21]. This protocol uses 1.5 M urea to keep the protein "soluble" in the supernatant after the initial centrifugation of the bacterial cell extracts. However, 1.5 M urea concentration is much lower than the midpoint of the urea-induced denaturation curve (approximately 5 M [22]), which indicates that there is no need to denature the IMPDH to "solubilize" it. We then hypothesized that IMPDH properly folds in the cytoplasm of *E. coli*; however, the high background concentration of macromolecules in the initial cell extracts favored the formation of large IMPDH assemblies that readily pelleted during a soft centrifugation.

We therefore tested the influence of macromolecular crowding on IMPDH filament assembly *in vitro* under different experimental conditions by monitoring protein assembly with turbidimetry. Our results showed that at high Ficoll-70 concentrations, both human IMPDH isoforms (HsIMPDH1 and HsIMPDH2) spontaneously assemble into large polymers, as indicated by the large increase in the turbidity of the solution (Fig. 3A and Supplemental Fig. 4A), and further corroborated by EM (upper panels of Fig. 3B and Supplemental Fig. 4B). At Ficoll-70 concentrations $\geq$150 mg/mL, most of the IMPDH is included within these polymers. These results led us to conclude that the formation of micron-length cytoophidia-like structures is due to the

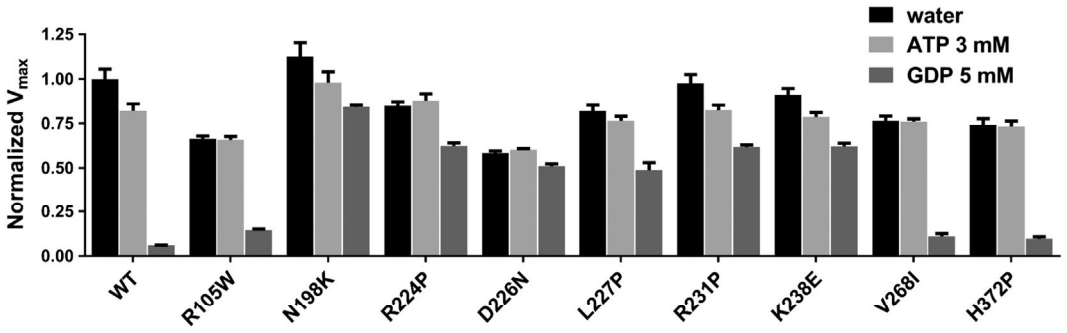

Fig. 2. Retinopathy-associated missense mutations disrupt GTP/GDP-mediated allosteric inhibition *in vitro*. Normalized catalytic activity (V_{max} derived from the Michaelis–Menten analysis of the experimental data) of HsIMPDH1-WT and retinopathy-associated mutants in the absence or presence of purine nucleotides. The error bars represent SEM.

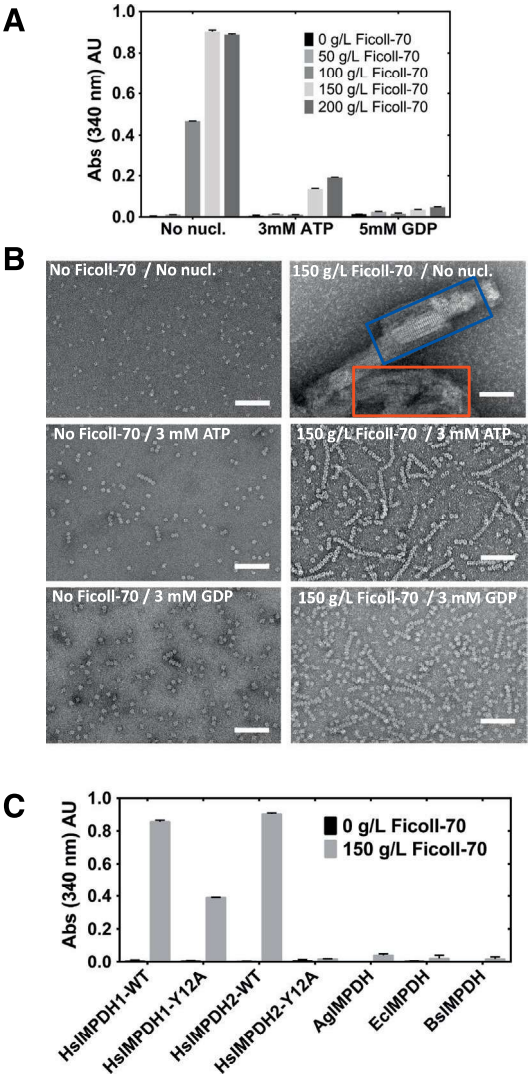

Fig. 3. *In vitro* reconstitution of human IMPDH cytoophidia assembly. (A) Turbidity measurements, indicating the formation of large polymers of HsIMPDH2, at different Ficoll-70 concentrations in the presence or absence of purine nucleotides. (B) EM analysis of the samples in the absence and presence Ficoll-70. The scale bars represent 100 nm. The red rectangle in the upper right panel shows bundles of twisted and curved filaments that intricate into the three dimensions without apparent regular or defined structure, while the blue rectangle shows ordered bundles of parallel protofilaments that were sporadically observed. (C) Turbidity measurements of purified IMPDH from different organisms. HsIMPDH1, *Homo sapiens* isoform 1; HsIMPDH2: *H. sapiens* isoform 2; AgIMPDH: *A. gossypii*; EcIMPDH: *E. coli*; BsIMPDH: *B. subtilis*. The error bars represent SEM.

macromolecular crowding conditions, since mesoscale polymerization can be detected neither at low crowding agent concentrations nor in its absence.

As a negative control, we used the Y12A missense mutation that has been previously reported to abrogate polymerization of HsIMPDH2 in cultured cells [5]. In accordance with this report, we were not able to detect significant assembly of the HsIMPDH2-Y12A mutant *in vitro* in dilute solutions or in crowding conditions (Fig. 3C). In contrast, we observed significant polymerization of the HsIMPDH1-Y12A mutant under macromolecular crowding conditions, although to a lower extent than the wild-type protein (Fig. 3C). These results agree with previous reports that describe a higher tendency to polymerize of HsIMPDH1 than HsIMPDH2 [23]. In addition, we tested whether the IMPDH enzymes from different organisms, other than humans, can also form cytoophidia-like polymers *in vitro*. Within Fig. 3C, it can be observed in that, in contrast to the two human isoforms, the eukaryotic *A. gossypii* (AgIMPDH), the bacterial *E. coli* (EcIMPDH) and *Bacillus subtilis* (BsIMPDH) enzymes are unable to form cytoophidia-like structures in our experimental conditions.

To further corroborate that eukaryotic AgIMPDH does not form cytoophidia, we ectopically overexpressed this gene in HeLa and HEK293T cells. As it is shown in Supplemental Fig. 4C, in contrast to HsIMPDH2 that showed a large amount of cytoophidia in essentially all the transfected cells, no detectable polymer formation was observed for AgIMPDH, despite the large amount of protein observed into the cytoplasm. Thereby, our results demonstrate that the ability of human IMPDH to form cytoophidia is not universal, since not all—eukaryotic or prokaryotic—IMPDH enzymes are able to assemble into large aggregates. In agreement with our results, other authors could neither find IMPDH polymers in the model yeast *Saccharomyces cerevisiae* [24].

The huge polymers of human IMPDH that formed *in vitro* under macromolecular crowding conditions are composed of octamers that associate into bundles of twisted and curved filaments that intricate into three dimensions without apparent regular or defined structure (red rectangle in the upper right panel of Fig. 3B and upper right panel of Supplemental Fig. 4B). Nonetheless, ordered bundles of parallel protofilaments were eventually observed within the huge polymers in some of the HsIMPDH2 micrographs (blue rectangle in the upper right panel in Fig. 3B). Direct distance measurements and power spectra analysis by fast Fourier transform of the protofilaments within these bundles showed a repetitive longitudinal spacing of 58.2 ± 0.4 Å. This longitudinal spacing is compatible with the expanded ATP-induced ~115-Å-long octamers previously observed by x-ray crystallography for AgIMPDH [6] and by SAXS for human IMPDH.

Remarkably, when ATP or GDP was present, the turbidity of the solution was significantly lower than in their absence (Fig. 3A and Supplemental Fig. 4A), indicating that these nucleotides inhibited the assembly of IMPDH into cytoophidia-like structures. The EM analysis of the polymers formed in the presence of purine nucleotides revealed either isolated octamers or

helical oligomers, extended for ATP and compacted for GDP (Fig. 3B and Supplemental Fig. 4B). A detailed analysis of the polymers formed in the presence of purine nucleotides can be found in the Supplemental Information, including the 3D reconstructions of ATP and GDP-induced protofilaments formed under macromolecular crowding conditions (Supplemental Fig. 5).

Moreover, once the cytoophidia-like polymers were spontaneously formed *in vitro*, the addition of either ATP or GDP depolymerized them, but the extent of this depolymerization strongly depended on the incubation time before nucleotide addition, that is, the maturation time [18]. The more mature the cytoophidia-like polymers are, the longer it takes to depolymerize them by GDP or ATP (Supplemental Fig. 6).

In summary, both human IMPDH isoforms spontaneously assemble *in vitro* into micron-length cytoophidia-like structures under macromolecular crowding conditions that resemble the cytoophidia found in cells. Under these conditions, the presence of purine nucleotides in the solution strongly reduces IMPDH cytoophidia formation, by both inhibiting assembly and inducing disassembly. Thus, our experimental setup reconstitutes *in vitro* the reversible guanine nucleotide-controlled cytoophidia assembly phenomenon previously reported to occur in cells. Our results also indicate a similar role for adenine nucleotides *in vitro*, although this observation remains to be corroborated *in vivo*.

Retinopathy-associated missense mutations in IMPDH1 alter the nucleotide-dependent cytoophidia dynamics *in vitro*

We next studied the nucleotide-dependent dynamics of the assembly of cytoophidia-like polymers *in vitro* for the HsIMPDH1 enzymes containing the retinopathy-associated mutations. All the mutants have the ability to spontaneously assembly into cytoophidia-like polymers to a similar extent than the wild-type enzyme (Fig. 4). Nonetheless, those mutants where the GTP/GDP allosteric inhibition is abrogated have also altered nucleotide-controlled regulation of cytoophidia-like assembly (Fig. 4) and disassembly (Supplemental Fig. 7A). The only exception is the mutant N198K that cannot be allosterically inhibited by GTP/GDP but possesses assembly dynamics comparable to the wild-type enzyme (Fig. 4 and Supplemental Fig. 7A). These data might indicate that the non-canonical guanine nucleotide binding site is needed for allosteric inhibition mediated by GTP/GDP, but is not implied in the regulation of assembly by nucleotides.

Remarkably, our data on cytoophidia-like structures assembled *in vitro* perfectly agree with a recent report that showed that HsIMPDH1 mutant enzymes R224P, D226N and R231P formed irreversible cytoophidia in transfected HEK293T cells when treated with guanosine [14].

IMPDH cytoophidia are catalytically active in vitro but more resistant to GTP/GDP inhibition

We next studied the effects of the polymerization into micron-length cytoophidia-like structures on the catalytic activity *in vitro.* To perform these experiments, we used as control the Y12A mutants that have compromised polymerization ability (Fig. 3C). Remarkably, we observed no significant differences between the catalytic activities of the Y12A mutants and the wild-type enzymes, neither in crowded nor in non-crowded solutions (Supplemental Table 2, Fig. 5A and B). The slight increase in the $K_{1/2}$ values between crowded and non-crowded conditions is most probably due to excluded volume and substrate limited diffusion effects, produced by the high concentrations of Ficoll-70. Indeed, similar differences in the $K_{1/2}$ values have

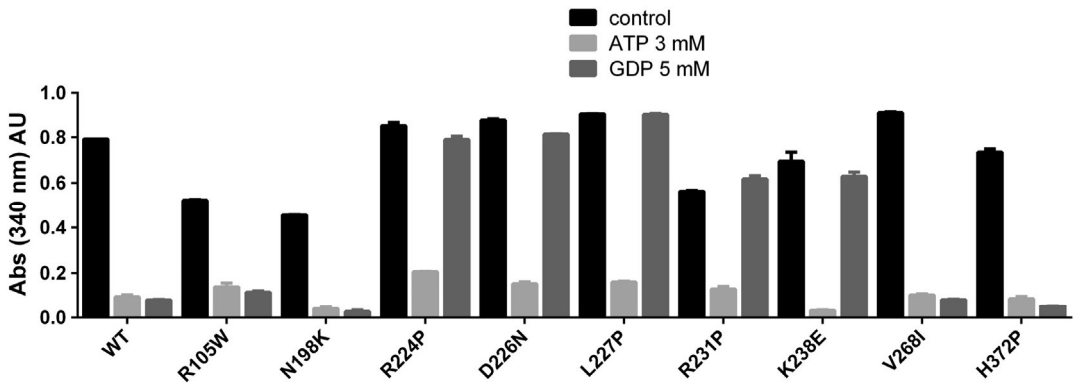

Fig. 4. Retinopathy-associated missense mutations alter IMPDH cytoophidia assembly *in vitro.* Turbidity measurements, indicating the formation of large polymers *in vitro*, at 150 g/L Ficoll-70 of HsIMPDH1 wild-type and retinopathy-associated mutants (0.25 mg/mL) in the absence or presence of purine nucleotides. Data were measured 10 min after dilution of the proteins into a solution containing Ficoll-70 and the indicated nucleotides. The error bars represent SEM.

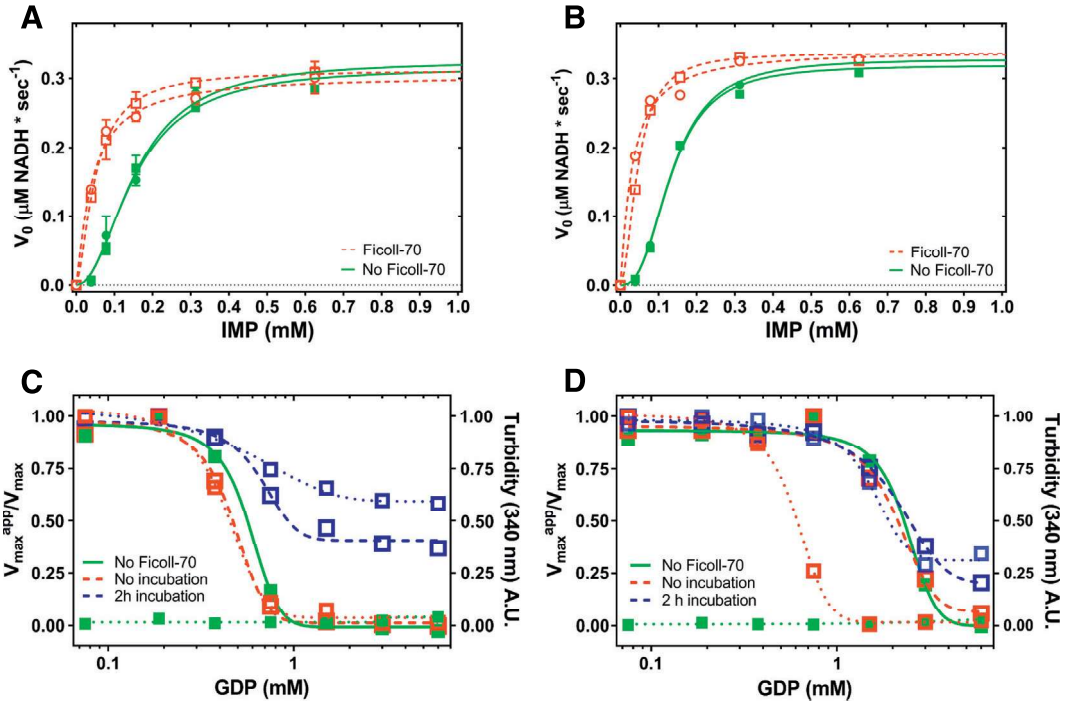

Fig. 5. Human IMPDH cytoophidia are catalytically active and resistant to GDP allosteric inhibition. (A and B) Michaelis–Menten representation of the catalytic activity of HsIMPDH1 (A) and HsIMPDH2 (B) wild-type (squares) and Y12A mutant (circles) in a dilute solution (solid figures and continuous green lines) and in the presence of 150 g/L Ficoll-70 (empty figures and discontinuous red lines). (C and D) Plots representing normalized solution turbidity (dotted lines) and catalytic activity (V_{max}^{app}/V_{max}; solid figures and continuous green line in the absence of Ficoll-70, empty figures and dashed red line for the short incubation with Ficoll-70, and empty figures and dashed blue line for the long incubation with Ficoll-70) at different GDP concentrations for HsIMPDH1-WT (C) and HsIMPDH2-WT (D). In our experimental setup, the measurements were performed approximately 30 min after GDP addition. Lines represent the non-linear regression analysis of the experimental data, according to a standard allosteric sigmoidal equation (GraphPad Prism). The error bars represent SEM.

been reported for a number of enzymes using similar crowding agents [25].

As an additional control, just before the measurements, we centrifuged the samples (5.000*g* for 10 min), so that the cytoophidia-like polymers were pelleted and the tetramers, octamers and small oligomers remained in the supernantant. The catalytic activity in the supernatant of the wild-type enzymes under crowding conditions was significantly reduced (Supplemental Fig. 7B), demonstrating that most of the catalytic activity comes from the IMPDH cytoophidia. In addition, most of the Y12A mutant enzyme that have compromised polymerization (Supplemental Fig. 7C) cannot be pelleted using these centrifugation conditions, therefore leaving the activity in the supernatant comparable to the activity prior to centrifugation (Supplemental Fig. 7B). From these experiments, we can conclude that IMPDH polymerization into micron-length cytoophidia-like structures did not significantly affect the catalytic activity in our *in vitro* experimental conditions.

Since GTP and GDP promote both cytoophidia disassembly and catalytic activity inhibition, it can be hypothesized that IMPDH polymerization might serve to fine-tune the allosteric regulation of the enzyme. To test this hypothesis, we studied how GDP affects the catalytic activity of the cytoophidia-like structures assembled in our *in vitro* system. As observed in Fig. 5C, non-mature polymers (without incubation before GDP addition) demonstrated inhibition of the catalytic activity while being depolymerized (red data) that showed no significant differences to the inhibition of the unassembled protein (green data). In contrast, the cytoophidia-like polymers that had been pre-incubated for 2 h before GDP addition, were more resistant to GDP-induced depolymerization (see also Supplemental Fig. 5) and, to a certain extent, were resistant to GDP allosteric inhibition (blue data). As expected, this behavior can also be observed for HsIMPDH2 but to a lesser extent (Fig. 5D), given that HsIMPDH2 is more sensitive to GDP-induced depolymerization than HsIMPDH1 (Supplemental Fig. 5). Moreover, HsIMPDH2 was depolymerized at lower GDP concentrations than those required to inhibit its catalytic activity (Fig. 5D). This observation agrees with the data presented above showing that GDP

induces octamer compaction at lower concentrations than those required for catalytic activity inhibition (Fig. 1D).

Discussion

Although there is wide knowledge on the enzymatic reaction mechanisms of IMPDH and its inhibition by a variety of molecules, there is an evident lack of information on its physiological mechanisms of regulation. Indeed, it has only been since the last few years that we have obtained the first experimental evidences on how the signal triggered by the binding of nucleotides to the regulatory Bateman domain is transmitted to the catalytic domain to modulate the enzymatic activity of IMPDH. To this respect, it has been recently described a conformational switch—controlled by purine nucleotides—that modulates the catalytic activity of eukaryotic IMPDH enzymes. The switch was first proposed by crystallography and x-ray scattering using the enzyme AgIMPDH from the industrial fungus *A. gossypii* [6] and was recently observed by EM with HsIMPDH2, the second isoform of human IMPDH [5]. We further demonstrate here that this conformational switch operates in both human IMPDH isoforms, suggesting that it might be conserved within all eukaryotic IMPDH enzymes. Moreover, a similar conformational switch, modulated by adenine nucleotides, has also been reported for some prokaryotic IMDPHs [2], despite the fact that these enzymes are not regulated by guanine nucleotides [7]. This observation suggests that the conformational switch is inherent to the acquisition of the Bateman regulatory domain, before the divergence of prokaryotic and eukaryotic enzymes. Nevertheless, the latter evolved separately to generate an additional non-canonical nucleotide binding site that allows the inhibition of the enzyme by GTP and GDP, the end products of the IMPDH's metabolic pathway.

Remarkably, we have found functional differences between the two human isoforms of IMPDH, where GTP/GDP-mediated allosteric inhibition of the catalytic activity is nicely correlated with octamer compaction in HsIMPDH1. In contrast, HsIMPDH2 octamer compaction occurs at lower GTP/GDP concentrations than those required for catalytic inhibition. These data, observed both in HsIMPDH2-Y12A (Fig. 1D) and HsIMPDH2-WT (Fig. 5D), indicate that additional features, other than octamer compaction itself, are required to inhibit HsIMPDH2. Possibly, the catalytic inhibition of IMPDH requires the binding of GTP/GDP to the three allosteric sites within the Bateman domain, while octamer compaction can happen with only a partial occupancy of these sites. Thereby, distinct affinities of GTP/GDP among the three nucleotide-binding sites of HsIMPDH1 and HsIMPDH2 might be the cause of the observed differences. In addition, our data show that HsIMPDH1 has a significantly higher tendency to filament than HsIMPDH2, in accordance with previous reports [23]. Future experimental studies will elucidate whether the different sensitivities to GTP/GDP-mediated allosteric inhibition and/or the different propensities to polymerize of the human IMPDH isoforms might have physiological consequences.

Presently, it is clearly accepted that the filamentation of enzymes to form cytoophidia serves as a general mechanism for the regulation of metabolism by fine-tuning protein functional and structural properties [12,13]. Indeed, enzyme filamentation seems to be rather extended with more than 20 metabolic enzymes reported to filament in *S. cerevisiae* [24]. Perhaps the most representative examples of cytoophidia-forming enzymes are those that catalyze the limiting steps in the *de novo* biosynthetic pathways of pyrimidine and purine nucleotides, CTPS and IMPDH, respectively.

Human CTPS filaments lock the enzyme into an active conformation, providing a mechanism for increasing the catalytic activity in response to metabolic state [26]. Similarly, human IMPDH cytoophidia formation correlates with rapid cell proliferation [11,14,15]; however, the *in vitro* reconstituted polymers show identical activity for both polymerized and non-assembled IMPDH [5]. In any case, the reported structural and functional data for IMPDH cytoophidia *in vitro* are based on polymers, induced by ATP or GTP, that are formed by the repeated back-to-back stacking of tetramers and octamers into single filaments [4,5], which do not represent the micrometer long and thick bundles observed in cells [10,19]. The results presented here demonstrate that these polymers do not represent cytoophidia but rather the remnants of their depolymerization. Our experimental conditions yield IMPDH polymer bundles *in vitro* with similar dimensions to the micron-length cytoophidia found in cells. Moreover, the dynamics of these polymers is modulated by guanine nucleotides *in vitro* in the same way as it has been observed in cells, as it will be discussed below. Thereby, our conditions allow a much better biochemical and structural characterization of this biological process.

The nucleotide-mediated steric self-compatibility of the Bateman interface and the highly symmetric structure of the octamers promote the assembly of IMPDH into the relatively thin and extended filaments that have been previously reported to form *in vitro* [4,5]. Nonetheless, once these filaments are formed, they are not able to significantly associate side by side to form the bundles that constitute cellular cytoophidia. The higher-order assembly into bundles of filaments proceeds only in the absence of nucleotides and seems to be a cooperative process, much less favorable than the nucleotide-induced single filament assembly is. Consistent with these observations, IMPDH assembly into micron-length cytoophidia-like structures depends on macromolecular crowding conditions, indicating that this assembly reaction is not only driven by enthalpy

due to specific interface interactions, but rather is also driven by entropy as a consequence of excluded volume effects [27]. Indeed, in a crowded *milieu*, oligomerization is greatly favored to minimize the overall crowding by enhancing protein association, which can thereby reduce the excluded volume [28]. The cytoophidia-like polymers assembled under these conditions are constituted by IMPDH octamers associated without an apparent order, although highly ordered specimens are also observed in the HsIMPDH2 micrographs. This observation indicates that the association of IMPDH octamers under crowding conditions confers high flexibility and dynamicity to the polymers, which is in further agreement with the observed variety of shapes that easily inter-convert in cells.

Our *in vitro* results reconstitute what it is observed in cells: IMPDH assemble into micron-length cytoophidia-like structures upon guanine nucleotide depletion but cytoophidia disassemble after guanine levels recover. This observation might also apply for the adenine nucleotides, because it is assumed that the levels of the adenine and guanine nucleotide pools rise or decrease in parallel, at least to a certain extent. Several mechanisms explain the parallel changes in adenine and guanine nucleotide levels. First, lowering the GTP levels might provoke a decrease in the adenine nucleotide levels through a dual action by (i) a reduced synthesis of AMP through adenylosuccinate synthetase, for which GTP serves as cofactor, and (ii) a greater degradation of AMP by AMP deaminase, which is inhibited by GTP. Second, an interplay exists between the syntheses of AMP/ATP and GMP/GTP from IMP, where ATP is required for the synthesis of GMP at the level of GMP synthase.

In addition, it will be interesting to study how the presence of substrates and products affect cytoophidia dynamics, as it has been very recently reported that the intracellular IMP accumulation promotes cytoophidia assembly, whereas elevated GTP level triggers the disassociation of aggregates [14]. Therefore, the balance GTP/IMP might be an additional important factor in regulating cytoophidia dynamics that definitively deserves to be investigated. For instance, it can be expected that IMP, bound to the active site, might somehow affect GTP-induced octamer compaction, given that this compaction implies the interaction of the finger domains, which place adjacent to—and interact with—the active site.

How do adenine and guanine nucleotides modulate IMPDH polymerization? A plausible explanation is that these nucleotides induce IMPDH octamer conformations that allow a few octamers to stack back-to-back and form short lineal filaments [4,5], but these filaments do not significantly associate laterally to form the large bundles that constitute the cytoophidia-like polymers. In contrast, in the absence of purine nucleotides, human IMPDH adopts a conformation that under crowding conditions favors both filament formation and filament bundling. A schematic representation of this hypothesis is shown in Fig. 6. In support of this hypothesis, three different conformations for eukaryotic IMPDHs have been reported (Fig. 6): (i) ATP-induced extended active octamers (5MCP, [6]), (ii) GTP/GDP-induced compacted inhibited octamers (6I0O, 6I0M in this work and 4Z87 [7]), and (iii) extended octamers with no nucleotide bound at the Bateman domain (1NF7 and 1NFB). The structures of the apo-enzyme and the ATP-induced IMPDH octamers have similar dimensions, but they significantly differ in the bending of the Bateman module that increases upon ATP binding (Fig. 6). Therefore, it is then tempting to speculate that the less bent Bateman module of the apo-enzyme octamers favors the lateral packing of the single filaments that result in large micrometric bundles. On the contrary, the increased bending of the Bateman module, induced by the binding of either ATP or GTP/GDP to the allosteric sites, avoids the lateral association of octamers and single protofilaments that consequently avoids the formation of cytoophidia-like structures (Fig. 6). Indeed, the crystal packing of 1NF7 (Supplemental Fig. 8A) would be compatible with the repetition pattern observed in the ordered bundles of HsIMPDH2 found in some of the micrographs of the *in vitro* reconstituted cytoophidia-like polymers (Fig. 3B) and in a previous report [19], suggesting that this crystal might be mimicking the packing of IMPDH within the cytoophidia.

Our results demonstrate that assembly into cytoophidia-like structures does not significantly change the catalytic activity of purified IMPDH *in vitro*. These results agree with a previous report that could neither find differences in catalytic activity between a mutant unable to polymerize (HsIMPDH2-Y12A) and the wild-type enzyme, both *in vitro* and in cultured cells [5]. In turn, IMPDH assembly modulates the sensitivity of the enzyme to allosteric inhibition. Remarkably, the more mature the cytoophidia-like polymers (longer incubation times) are, the more resistant to GTP/GDP-induced octamer compaction they become and thereby more resistant to depolymerization and subsequent inhibition of the catalytic activity. In other words, the more mature a cytoophidia-like polymer is, the longer it takes to depolymerize by GTP/GDP. At this point, it remains unknown how maturation time correlates to resistance to GDP-induced octamer compaction *in vitro*, but it is clear that it might have important physiological implications. The longer a cell remains in a state of guanine nucleotide deprivation, the longer it will take to recover, that is, the longer IMPDH should work actively in the absence of negative feedback inhibition. Therefore, IMPDH cytoophidia formation and maturation might constitute a mechanism to temporal and spatially regulate the ability of IMPDH polymers to maintain especially high intracellular levels of guanine nucleotides when required, for example, for active cell proliferation or after a pharmacological depletion of the guanine nucleotide pools. At this point, it is important to

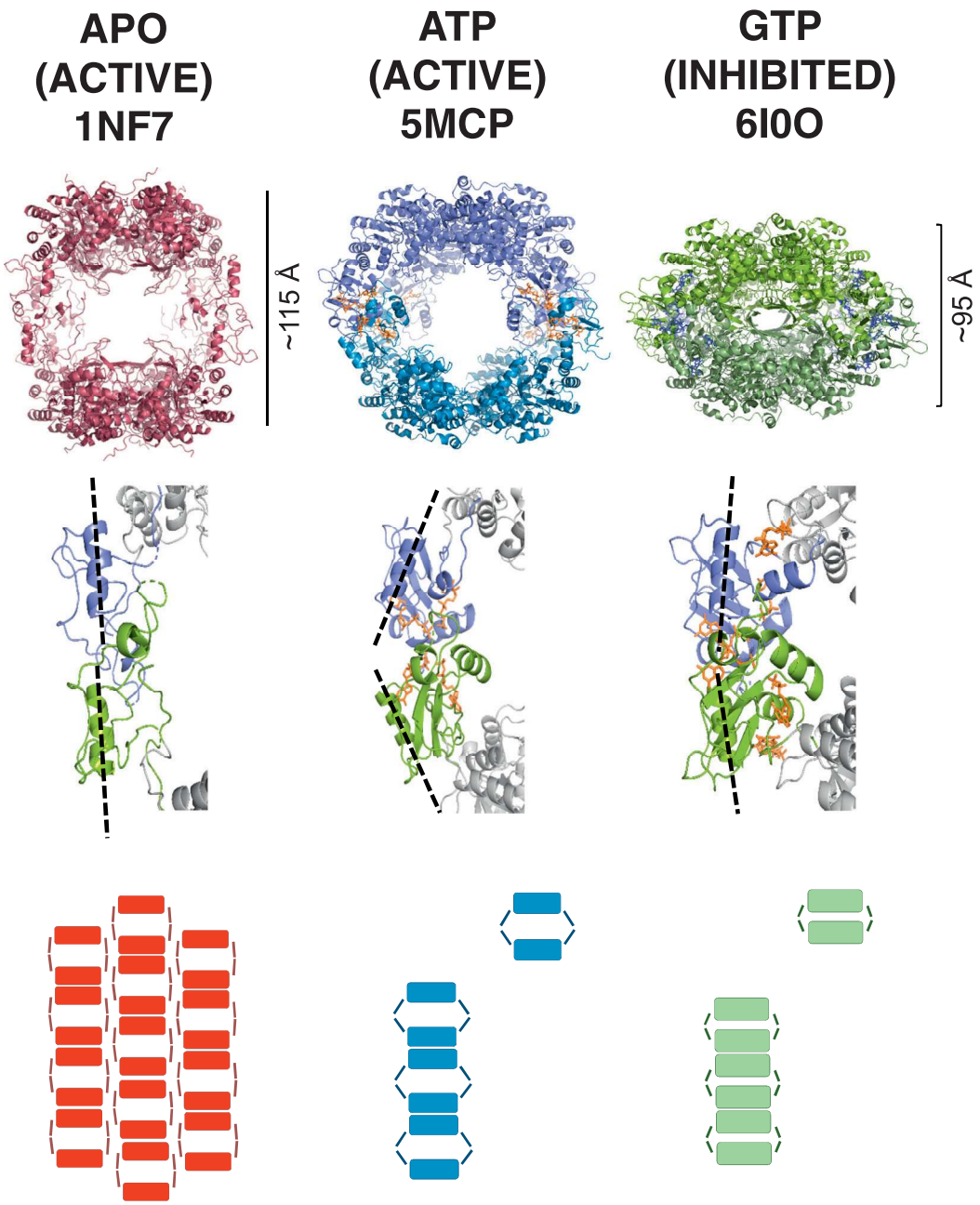

Fig. 6. The nucleotide controlled-conformational switch of human IMPDH. Upper panels: the three different octamer conformations observed in eukaryotic IMPDH enzymes and their respective PDB codes. IMPDH protein is shown in cartoons and nucleotides in sticks. The approximate longitudinal dimensions of the octamers are indicated on their side. Middle panels: close-up view of two interacting Bateman domains from adjacent tetramers within the octameric arrangement. The black dashed lines show the approximate longitudinal axis of helices comprising residues 194–204. Lower panels: schematic representation of the assembly of human IMPDH into different polymers.

stress that this study was performed *in vitro*, from purified components, but it is envisaged that *in vivo* post-translational modifications and interaction partners will play an important role in the regulation of the dynamics of IMPDH cytoophidia assembly.

Finally, we demonstrate that the mutations in HsIMPDH1 associated with human retinopathies map into the allosteric nucleotide binding sites, which therefore alter the nucleotide-controlled conformational switch. Subsequently, they also disrupt allosteric inhibition mediated by GTP/GDP and modify the dynamics of the cytoophidia-like polymers *in vitro*. Thereby, our data indicate that the HsIMPDH1 mutations within the first instance will affect the intracellular

levels of the purine nucleotide pools in retinal cells that, in a medium/long term, will lead to visual receptor cell death and subsequent retinal degeneration. Future studies are needed to elucidate the molecular details on how the alterations in the nucleotide pools develop into retinopathies. Moreover, it will also be very interesting to explore the potential physiological roles that cytoophidia play in retinal development. Indeed, in preliminary experiments, we were able to detect IMPDH cytoophidia in the retina of adult mice as 1- to 2-μm-long structures, mostly localized in the periphery of the retina, although they were detected throughout this organ (Supplemental Fig. 8B). Altogether, these data indicate that cytoophidia form in the retina *in vivo* under normal developmental conditions and suggest a potential physiological role of cytoophidium that might be altered by the retinopathy-associated missense mutations of human IMPDH1.

The data presented in this manuscript show that the effective concentrations of GDP that affect the IMPDH conformational switch, the polymerization dynamics, and the inhibition of the catalytic activity, lie roughly in the same range than the expected intracellular GTP/GDP concentrations, this is, in the 0.1- to 1-mM range [29]. Therefore, our *in vitro* data suggest that the molecular mechanisms we propose might be relevant *in vivo* at the expected physiological intracellular nucleotide concentrations, although this hypothesis awaits experimental confirmation.

In summary, our results provide novel and valuable information for understanding the physiological regulation of IMPDH as well as deciphering the putative roles of IMPDH cytoophidia *in vivo*, both under physiological and pathological conditions. Moreover, given that IMPDH is a widely validated drug target in several types of diseases, the reported results might eventually support future studies to determine the therapeutic potential of the cytoophidium as a useful target and/or biomarker.

Materials and Methods

Proteins and nucleotides

Expression and purification of IMPDH proteins was performed as previously described [7,21]. Nucleotides were purchased from Sigma-Aldrich and Jena Bioscience. Missense mutations were introduced into the bacterial expression vectors by using QuickChange II Site-directed mutagenesis protocol (Agilent Technologies).

Protein polymerization analysis *in vitro*

In vitro polymerization was monitored by turbidimetry at 340 and 410 nm on a spectrophotometer by using proteins, purified to homogeneity, at a concentration of 0.1–0.25 mg/mL in buffer 100 mM Tris–HCl, 100 mM KCl, 2 mM DTT and 1 mM $MgCl_2$ (final free Mg^{+2} concentration; pH 8.0) and in the presence of the indicated amounts of Ficoll-70 and/or nucleotides.

Control experiments were also performed by pelleting the polymers by centrifugation and determining the protein concentration in pellets and supernatants by spectrophotometry and/or SDS-PAGE densitometry. Samples of protein polymers were taken from each experiment for further analysis by EM (see below).

Enzyme kinetics assay

IMPDH activity was assayed, as previously reported [6], at 32 °C using 96 or 384-well microtiter plates by monitoring the reduction of NAD^+ and the subsequent increase in absorbance at 340 nm. All the enzyme kinetics and inhibition experiments were performed by using a fixed concentration of enzyme (100 μg/mL) and NAD^+ (0.5 mM), while IMP varied from 0.04 to 5 mM. The reaction buffer was 100 mM Tris–HCl, 100 mM KCl, 2 mM DTT and 1 mM $MgCl_2$ (final free Mg^{+2} concentration; pH 8.0).

Initial velocities (V_0) were extracted from the time-course reaction progress curves, which were then fitted by non-linear regression analysis to an allosteric sigmoidal equation using GraphPad Prism (GraphPad Prism Software, Inc.) to estimate the $K_{1/2}$ and V_{max} values. It must be stated here that, given the high concentration of enzyme used for these experiments, the steady state in the lowest substrate concentrations cannot be ensured, which might influence the precision of the calculated $K_{1/2}$ values.

To monitor enzyme kinetics under macromolecular crowding conditions, where turbidity might interfere with the measurement at λ = 340 nm, the catalytic reaction was stopped by incubating the samples with 4 M urea (final concentration) to disaggregate protein assemblies and avoid the turbidity of the solution. These experiments demonstrated that the constant background at λ = 340 nm due to the presence of turbidity in the solution could be easily subtracted from the raw measurements, without affecting the precise estimation of the kinetic parameters.

For control experiments, HsIMPDH1/2-WT and HsIMPDH1/2-Y12A mutant enzymes under macromolecular crowding conditions were centrifuged at 5000*g* for 10 min at 25 °C, to pellet the cytoophidia-like polymers, and the catalytic activity of the supernatants was measured as described above.

SAXS

SAXS measurements were performed at the B21 beamline at the Diamond Light Source. Protein samples at 2.5 mg/mL in buffer 20 mM Tris–HCl, 300 mM KCl, 1 mM $MgCl_2$ (final free Mg^{+2} concentration) and 3 mM DTT (pH 8.0) were measured in the presence of increasing amounts of nucleotides (total concentration of nucleotides ranging from 0.02 to

3 mM). Experimental data were reduced following standard methodologies by using the program PRIMUS. The fractions of tetramers, and expanded and compacted octamers were calculated with the program OLIGOMER and the theoretical solution scattering profiles with CRYSOL. All these programs are found within the ATSAS software suite [30].

Crystallization and structure determination

Crystals of the complexes HsIMPDH2-GTP and HsIMPDH2-GDP were grown at 22 °C using the vapor diffusion method by mixing a protein solution at 7.5 mg/mL in 10 mM Tris–HCl, 150 mM KCl, 1 mM DTT, 7.5 mM GTP (or GDP) and 5 mM total $MgCl_2$ (pH 8.0), with an equal volume of mother liquor consisting of 25% PEG-1500 and 0.1 M buffer MIB (malonic acid, imidazole and boric acid) at pH 9.0 for HsIMPDH-GTP and 0.1 M sodium citrate at pH 5.5, 0.2 M lithium sulfate and 15% ethanol for HsIMPDH2-GDP. Protein crystals were flashed-cooled in liquid nitrogen, and data were collected at 100 K, using monochromatic x-rays of ≈1 Å wavelength, at the MX beamlines of the Diamond Light Source synchrotron (UK) or the XALOC beamline in the ALBA synchrotron (Spain). Crystals of HsIMPDH2-GDP were cryo-protected by immersion in NVH oil before being flashed-cooled in liquid nitrogen. Diffraction intensities were indexed and integrated by using the software autoPROC [31].

The experimental data were phased by molecular replacement using the program PHASER [32] using as template the structure of the complex AgIMPDH-GDP (PDB code 4Z87). The structures were iteratively refined by alternating manual modeling with COOT [33] with the automated refinement utility of the PHENIX crystallographic software suite [34]. Rigid body, gradient-driven positional, restrained individual isotropic B-factor and TLS were used for structure refinement.

EM

Samples were analyzed by EM after being adsorbed to glow-discharged carbon coated grids and stained with 2% uranyl acetate. Grids were observed using a JEOL JEM-1230 transmission electron microscope operated at 100 kV and a nominal magnification of 40.000. Images were taken under low-dose conditions with a CMOS Tvips TemCam-F416 camera, at 2.84 Å per pixel. Image processing was performed using SCIPION package [35]. The contrast transfer function of the microscope for each micrograph was estimated using CTFFIND4 [36]. Helical segments were picked from the micrographs using the Xmipp3 manual-picking routine implemented inside SCIPION.

In the initial step, images of the helical segments were extracted and horizontally pre-aligned using a multi-reference pattern-free alignment protocol [37]. After pre-alignment, images were two-dimensional classified using RELION software [38] limiting in-plane rotations, allowing bimodal search and using a rectangular mask to focus the classification process in the helix. Classes containing the straightest particles were selected for 3D reconstruction. Initial model was built by assigning random rotation angles to the images and 3D reconstructed. This procedure generates featureless tubular structures suitable as a starting model for 3D classification in RELION; this classification was performed with no symmetry application to avoid initial bias in the reconstructions. Afterward, the selected classes were also refined without the application of helical symmetry. When the angular assignment of the images reached convergence, symmetry parameters of the volumes were determined using the "xmipp_volume_find_symmetry" utility and applied. Finally, a new cycle of refinement, applying symmetry, was carried out to generate the final structures.

Figures of protein structures, electron density maps and EM maps were rendered by using PyMOL (The PyMOL Molecular Graphics System, Version 2.0 Schrödinger, LLC).

Immunofluorescence

HeLa cells were grown onto poly-L-Lysine coated glass coverslips and fixed with 2.5% paraformaldehyde for 30 min at room temperature, washed three times with PBS, permeabilized for 10 min with Triton 0.1% X100 and blocked with 1% BSA for another 10 min. The primary antibody (mouse anti-HA 12CA5, Roche) was used at a 1:5000 dilution and incubated for 2 h at room temperature. The secondary antibody (Alexa-488 anti-mouse) was used at a 1:2000 dilution and incubated overnight at 4 °C. Cells were then washed with 1% BSA, and the nuclei were stained with DAPI.

Mice retinas were fixed by immersion in 4% paraformaldehyde for 4 h at 4 °C. The tissue was cryo-protected in 30% sucrose and embedded in OCT, and 16-μm sections were obtained. Sections were washed in PBS and blocked with 5% BSA, 2% goat serum and 0.1% Triton X100. Primary antibody (IMPDH, H-300; Santa Cruz; sc-50510) was incubated at a 1:30 dilution overnight at 4 °C and detected with a secondary antibody anti-rabbit Alexa-488 used at a 1:300 dilution, for 1 h at room temperature. Nuclei were stained with DAPI.

Accession numbers

The atomic coordinates and the structure factors described in this work have been deposited in the Research Collaboratory for Structural Bioinformatics Protein Data Bank under the codes PDB ID: 6I0O (HsIMPDH2-GTP) and PDB ID: 6I0M (HsIMPDH2-GDP). The EM-derived maps have been deposited in the Electron Microscopy Data Bank under the accession codes EMD ID: 4402 (HsIMPDH1-GDP) and EMD ID: 4403 (HsIMPDH1-ATP).

Acknowledgments

This work was supported by the Spanish Ministerio de Ciencia, Innovación y Universidades (grants BFU2016-79237-P to R.M.B. and BIO2014-56930-P to J.L.R.). D.F.J. was supported by a pre-doctoral contract from the "Junta de Castilla y León". We thank María Dolores Sánchez, Silvia Domínguez and Marta Santos for excellent technical help; Ángel Hernández for help with cell cultures; and Germán Rivas, José M de Pereda and Kyle B del Valle for their valuable comments and suggestions to the manuscript. Protein crystallography experiments were performed at the i03 beamline (Diamond Light Source, UK) and XALOC (ALBA Synchrotron, Spain) beamlines with the collaboration of Diamond and ALBA staff. X-ray scattering experiments were performed at the B21-Solution State SAXS beamline (Diamond Light Source, UK).

Appendix A. Supplementary data

Supplementary data to this article can be found online at https://doi.org/10.1016/j.jmb.2019.01.020.

Received 12 November 2018;
Received in revised form 9 January 2019;
Accepted 10 January 2019
Available online 18 January 2019

Keywords:
IMP dehydrogenase;
cytoophidia;
conformational switch;
allosteric regulation;
x-ray crystallography and scattering

Present address: E.M. Soriano, Institute for Cardiovascular and Metabolic Research, School of Biological Sciences, Harborne building, University of Reading, Whiteknights, Reading, RG6 6AS, United Kingdom.

Abbreviations used:
IMPDH, inosine 5′-monophosphate dehydrogenase; CTPS, CTP synthase; HsIMPDH2, isoform 2 of human IMPDH; SAXS, small-angle x-ray solution scattering; EM, electron microscopy; HsIMPDH1, isoform 1 of human IMPDH.

References

[1] L. Hedstrom, IMP dehydrogenase: structure, mechanism, and inhibition, Chem. Rev. 109 (2009) 2903–2928.
[2] G. Labesse, T. Alexandre, L. Vaupré, I. Salard-Arnaud, J. Him, B. Raynal, et al., MgATP regulates allostery and fiber formation in IMPDHs, Structure 21 (2013) 975–985.
[3] G. Labesse, T. Alexandre, M. Gelin, A. Haouz, H. Munier-Lehmann, Crystallographic studies of two variants of *Pseudomonas aeruginosa* IMPDH with impaired allosteric regulation, Acta Crystallogr. D Biol. Crystallogr. 71 (2015) 1890–1899.
[4] Y. Ji, J. Gu, A. Makhov, J. Griffith, B. Mitchell, Regulation of the interaction of inosine monophosphate dehydrogenase with mycophenolic acid by GTP, J. Biol. Chem. 281 (2006) 206–212.
[5] S.A. Anthony, A.L. Burrell, M.C. Johnson, K.C. Duong-Ly, Y.M. Kuo, J.C. Simonet, et al., Reconstituted IMPDH polymers accommodate both catalytically active and inactive conformations, Mol. Biol. Cell 28 (2017) 2600–2608.
[6] R.M. Buey, D. Fernandez-Justel, I. Marcos-Alcalde, G. Winter, P. Gomez-Puertas, J.M. de Pereda, et al., A nucleotide-controlled conformational switch modulates the activity of eukaryotic IMP dehydrogenases, Sci. Rep. 7 (2017) 2648.
[7] R.M. Buey, R. Ledesma-Amaro, A. Velazquez-Campoy, M. Balsera, M. Chagoyen, J.M. de Pereda, et al., Guanine nucleotide binding to the Bateman domain mediates the allosteric inhibition of eukaryotic IMP dehydrogenases, Nat. Commun. 6 (2015) 8923.
[8] D.A. McGrew, L. Hedstrom, Towards a pathological mechanism for IMPDH1-linked retinitis pigmentosa, Adv. Exp. Med. Biol. 723 (2012) 539–545.
[9] A.M. Pedley, S.J. Benkovic, A new view into the regulation of purine metabolism: the purinosome, Trends Biochem. Sci. 42 (2017) 141–154.
[10] W.C. Carcamo, M. Satoh, H. Kasahara, N. Terada, T. Hamazaki, J.Y. Chan, et al., Induction of cytoplasmic rods and rings structures by inhibition of the CTP and GTP synthetic pathway in mammalian cells, PLoS One 6 (2011), e29690.
[11] C.C. Chang, W.C. Lin, L.M. Pai, H.S. Lee, S.C. Wu, S.T. Ding, et al., Cytoophidium assembly reflects upregulation of IMPDH activity, J. Cell Sci. 128 (2015) 3550–3555.
[12] G.N. Aughey, J.L. Liu, Metabolic regulation via enzyme filamentation, Crit. Rev. Biochem. Mol. Biol. 51 (2015) 282–293.
[13] H. Wang, Q.-X. Saho, The cytoophidium: a novel intracellular compartmentation formed by metabolic enzymes, Acad. J. Biotechnol. 5 (2017) 7.
[14] G.D. Keppeke, C.C. Chang, M. Peng, L.Y. Chen, W.C. Lin, L.M. Pai, et al., IMP/GTP balance modulates cytoophidium assembly and IMPDH activity, Cell Div 13 (2018) 5.
[15] K.C. Duong-Ly, Y.M. Kuo, M.C. Johnson, J.M. Cote, J.M. Kollman, J. Soboloff, et al., T cell activation triggers reversible inosine-5′-monophosphate dehydrogenase assembly, J. Cell Sci. 131 (2018).
[16] S.J. Calise, W.C. Carcamo, C. Krueger, J.D. Yin, D.L. Purich, E.K. Chan, Glutamine deprivation initiates reversible assembly of mammalian rods and rings, Cell. Mol. Life Sci. 71 (2014) 2963–2973.
[17] S.J. Calise, D.L. Purich, T. Nguyen, D.A. Saleem, C. Krueger, J.D. Yin, et al., 'Rod and ring' formation from IMP dehydrogenase is regulated through the one-carbon metabolic pathway, J. Cell Sci. 129 (2016) 3042–3052.
[18] C.C. Chang, G.D. Keppeke, L.Y. Sung, J.L. Liu, Interfilament interaction between IMPDH and CTPS cytoophidia, FEBS J. 285 (2018) 3753–3768.
[19] P. Juda, J. Smigova, L. Kovacik, E. Bartova, I. Raska, Ultrastructure of cytoplasmic and nuclear inosine-5′-monophosphate dehydrogenase 2 "rods and rings" inclusions, J. Histochem. Cytochem. 62 (2014) 739–750.

[20] J.L. Liu, The cytoophidium and its kind: filamentation and compartmentation of metabolic enzymes, Annu. Rev. Cell Dev. Biol. 32 (2016) 349–372.
[21] E. Thomas, J. Gunter, J. Webster, N. Schieber, V. Oorschot, R. Parton, et al., Different characteristics and nucleotide binding properties of inosine monophosphate dehydrogenase (IMPDH) isoforms, PLoS One 7 (12) (2012).
[22] E. Nimmesgern, T. Fox, M.A. Fleming, J.A. Thomson, Conformational changes and stabilization of inosine 5′-monophosphate dehydrogenase associated with ligand binding and inhibition by mycophenolic acid, J. Biol. Chem. 271 (1996) 19421–19427.
[23] J.H. Gunter, E.C. Thomas, N. Lengefeld, S.J. Kruger, L. Worton, E.M. Gardiner, et al., Characterisation of inosine monophosphate dehydrogenase expression during retinal development: differences between variants and isoforms, Int. J. Biochem. Cell Biol. 40 (2008) 1716–1728.
[24] Q.J. Shen, H. Kassim, Y. Huang, H. Li, J. Zhang, G. Li, et al., Filamentation of metabolic enzymes in *Saccharomyces cerevisiae*, J. Genet. Genomics 43 (2016) 393–404.
[25] T. Vopel, G.I. Makhatadze, Enzyme activity in the crowded milieu, PLoS One 7 (2012), e39418.
[26] E.M. Lynch, D.R. Hicks, M. Shepherd, J.A. Endrizzi, A. Maker, J.M. Hansen, et al., Human CTP synthase filament structure reveals the active enzyme conformation, Nat. Struct. Mol. Biol. 24 (2017) 507–514.
[27] G. Rivas, A.P. Minton, Macromolecular crowding in vitro, in vivo, and in between, Trends Biochem. Sci. 41 (2016) 970–981.
[28] A.P. Minton, The influence of macromolecular crowding and macromolecular confinement on biochemical reactions in physiological media, J. Biol. Chem. 276 (2001) 10577–10580.
[29] T.W. Traut, Physiological concentrations of purines and pyrimidines, Mol. Cell. Biochem. 140 (1994) 1–22.
[30] D. Franke, M.V. Petoukhov, P.V. Konarev, A. Panjkovich, A. Tuukkanen, H.D.T. Mertens, et al., ATSAS 2.8: a comprehensive data analysis suite for small-angle scattering from macromolecular solutions, J. Appl. Crystallogr. 50 (2017) 1212–1225.
[31] C. Vonrhein, C. Flensburg, P. Keller, A. Sharff, O. Smart, W. Paciorek, et al., Data processing and analysis with the autoPROC toolbox, Acta Crystallogr. D Biol. Crystallogr. 67 (2011) 293–302.
[32] A.J. McCoy, R.W. Grosse-Kunstleve, P.D. Adams, M.D. Winn, L.C. Storoni, R.J. Read, Phaser crystallographic software, J. Appl. Crystallogr. 40 (2007) 658–674.
[33] P. Emsley, B. Lohkamp, W.G. Scott, K. Cowtan, Features and development of Coot, Acta Crystallogr. D Biol. Crystallogr. 66 (2010) 486–501.
[34] P.D. Adams, P.V. Afonine, G. Bunkoczi, V.B. Chen, I.W. Davis, N. Echols, et al., PHENIX: a comprehensive Python-based system for macromolecular structure solution, Acta Crystallogr. D Biol. Crystallogr. 66 (2010) 213–221.
[35] J.M. de la Rosa-Trevin, A. Quintana, L. Del Cano, A. Zaldivar, I. Foche, J. Gutierrez, et al., Scipion: a software framework toward integration, reproducibility and validation in 3D electron microscopy, J. Struct. Biol. 195 (2016) 93–99.
[36] A. Rohou, N. Grigorieff, CTFFIND4: fast and accurate defocus estimation from electron micrographs, J. Struct. Biol. 192 (2015) 216–221.
[37] C.O. Sorzano, J.R. Bilbao-Castro, Y. Shkolnisky, M. Alcorlo, R. Melero, G. Caffarena-Fernandez, et al., A clustering approach to multireference alignment of single-particle projections in electron microscopy, J. Struct. Biol. 171 (2010) 197–206.
[38] S.H. Scheres, RELION: implementation of a Bayesian approach to cryo-EM structure determination, J. Struct. Biol. 180 (2012) 519–530.